

Dealing with mismatched fMRI activations in fMRI constrained EEG cortical source imaging: a simulation study assuming various mismatch types

Chang-Hwan Im

Received: 20 July 2006 / Accepted: 10 December 2006 / Published online: 3 January 2007
© International Federation for Medical and Biological Engineering 2007

Abstract Although fMRI constrained EEG source imaging could be a promising approach to enhancing both spatial and temporal resolutions of independent fMRI and EEG analyses, it has been frequently reported that a hard fMRI constraint may cause severe distortion or elimination of significant EEG sources when there are distinct mismatches between fMRI activations and EEG sources. If estimating actual EEG source locations is important and fMRI prior information is used as an auxiliary tool to enhance the concentration of widespread EEG source distributions, it is reasonable to weaken the fMRI constraint when significantly mismatched sources exist. The present study demonstrates that the mismatch problem may be partially solved by extending the prior fMRI activation regions based on the conventional source imaging results. A hard fMRI constraint is then applied when there is no distinct mismatch, while a weakened fMRI constraint is applied when there are significant mismatches. A preliminary simulation study assuming different types of mismatches such as fMRI invisible, extra, and discrepancy sources demonstrated that this approach can be a promising option to treat mismatched fMRI activations in fMRI constrained EEG source imaging.

Keywords EEG source imaging · Multimodal neuroimaging · Inverse problem · Functional magnetic

resonance imaging (fMRI) · Electroencephalography (EEG)

1 Introduction

Temporal resolution of functional magnetic resonance imaging (fMRI) is highly limited due to relatively slow hemodynamic responses in spite of its excellent spatial resolution. On the contrary, electroencephalography (EEG) and magnetoencephalography (MEG) have superior temporal resolutions compared to fMRI, allowing studies of the dynamics of neural networks that occur on the order of tens of milliseconds. However, the spatial resolution of EEG and MEG do not match that of fMRI due to their limited number of sensors and ambiguity in the electromagnetic inverse problem [8]. Therefore, many researchers have attempted to combine the two different modalities to estimate brain functional activations with enhanced spatial and temporal resolutions.

An equivalent current dipole (ECD) model can be an option for the multimodal data fusion. The most widely used approach is to place small numbers of rotating dipole sources in fMRI activation foci and localize them using nonlinear fitting algorithms [1, 24, 25, 43]. Opitz et al. [33] and Torquati et al. [40] constrained the dipole locations and/or orientations based on the anatomical and functional priors, and then investigated temporal changes of the dipoles. These simple combinations of multimodal data can solve conventional problems of the ECD model in that the numbers and initial locations of the ECDs cannot be estimated *a priori*. However, these approaches still have some potential problems. If single dipoles are

C.-H. Im (✉)
Department of Biomedical Engineering, Yonsei University,
234 Maeji-ri, Heungeop-myun, Wonju-si
Kangwon-do 220-710, South Korea
e-mail: ich@yonsei.ac.kr

placed at each focus of fMRI activation, the discrete dipoles may not properly represent the large spatial extent of some activation [12, 41]. Moreover, it was observed in some simulation studies that constraining multiple dipole sources in all possible fMRI activation foci might yield considerable error if some ECD locations were not correctly estimated [12, 27].

Contrary to the ECD model, the distributed source model, sometimes called EEG/MEG source imaging, assumes many current dipoles scattered in source spaces, and then estimates the orientations and/or strengths of the dipoles using linear or nonlinear estimation methods. Based on this basic idea, Dale and Sereno [6] first proposed constraining the source space into anatomically known locations (interface between white and gray matter of the cerebral cortex extracted from an MRI) and orientations (perpendicular to the cortical surface), and then weighting the estimate based on *a priori* information. The distributed source approaches can be readily incorporated with fMRI data. The most straightforward way to impose the fMRI constraint upon the distributed source reconstruction is to restrict the possible source spaces to locations exceeding a threshold predetermined for fMRI statistical analyses [14, 35]. According to Liu et al.'s study [27], however, the results of this approach are very sensitive to generators of EEG or MEG signals that are not detected by fMRI. They also revealed that such distortion or misidentification could be considerably reduced by giving a constant weighting factor to the diagonal terms of the source covariance matrix in a linear inverse operator. They demonstrated from Monte-Carlo simulations that the optimal fMRI weighting for the non-activation regions should be 10% of that for the activation regions, in order to minimize the distortion. Some groups have used different weighting values, e.g., Wagner et al. [43] and Babiloni et al. [3], but their basic concepts are still the same as that of the previous study [27] in that they also gave different weighting factors to sources inside and outside the fMRI activation regions.

When using such fMRI constrained EEG or MEG source imaging, the widespread EEG/MEG source distribution can be spatially more focalized. Moreover, the use of the fMRI prior information can reduce spurious or phantom sources generated due to the *ill-posedness* of EEG/MEG inverse problems. On the other hand, the EEG or MEG can provide temporal information for the static fMRI results [5, 8, 26–28].

In practice, however, there frequently exist severe mismatches between fMRI and EEG/MEG sources [34, 42]. These mismatches are bound to occur due to the limited spatial sensitivity pattern of EEG/MEG

sensors and the limited time resolution of fMRI [2, 15].

The fMRI mismatched activations can be classified into three types: fMRI extra sources, fMRI invisible sources, and fMRI discrepancy sources. Some source activity may be located or oriented such that there is little electromagnetic field outside of the head. Examples of this are radially oriented sources in MEG and deep *closed field* sources in EEG, for which the activity patterns are such that the total macroscopic current is cancelled out. All of these examples could generate significant fMRI activation, but not in EEG or MEG. Furthermore, the fMRI activations can be detected where there are no neuronal activities because the fMRI signal is sensitive to parameters reflecting energy consumption [36], e.g., neurotransmitter release and uptake, vesicular recycling, and maintenance of membrane potentials. These kinds of sources are usually referred to as 'fMRI extra sources', which have been generally ignored in many studies due to their slight effect on the fMRI constrained source estimates [2]. On the other hand, some actual EEG/MEG sources cannot be detected in fMRI, which have been referred to as 'fMRI invisible sources'. Some neuronal sources, which are active only for a short time period, may be detected in EEG or MEG, but do not appear in fMRI results since fMRI integrates brain activity over time. The other type of mismatches, fMRI discrepancy sources, originates from an intrinsic discrepancy between fMRI and EEG/MEG due to the fundamental difference between hemodynamic and electrophysiological processes [5, 9, 31].

The crucial problem here is that the fMRI constrained EEG inverse solutions are still sensitive to the existence of such significant mismatches when the conventional weighting approaches are applied [2, 21, 29], and the mismatches may cause severe distortions or eliminations of meaningful neuronal sources.

Therefore, if one aims to identify the actual EEG source locations and uses the fMRI prior information as an auxiliary tool to enhance the concentration of the widespread EEG source distributions, it may be a better choice not to use the fMRI constraint when severe mismatches between fMRI and EEG sources are observed [15, 42].

The present study demonstrates that the mismatch problem may be partially solved by extending the prior fMRI activation regions based on the conventional source imaging results. When there are significant EEG sources lying outside fMRI activation regions, the prior regions are automatically expanded to include the missing EEG sources into the prior activation regions. Although some loss of focality in the resultant

EEG source images is inevitable, we can estimate more plausible EEG source locations instead. The use of this new approach rarely affects the results of fMRI constrained EEG source imaging if no major mismatch between the two modalities is detected; on the other hand, the new results become similar to those of conventional EEG source imaging without fMRI constraint if the mismatch level is significant. A preliminary simulation study performed by the author showed that this new approach may be useful to correct some discrepancy sources [22]. In the present study, the feasibility of the approach is verified more systematically using various simulations with artificially constructed EEG data assuming different kinds of mismatches such as fMRI invisible, extra, and discrepancy sources.

2 Methods

2.1 Forward and inverse methods

Since synchronously activated pyramidal cortical neurons, which are oriented perpendicularly on the cortical surface, are widely believed to be the main EEG and MEG generators, many recent studies have adopted this physiological phenomenon as a basic anatomical constraint in EEG or MEG source imaging [3, 4, 6, 8, 23]. To impose the anatomical constraint, many dipolar sources were placed on the cortical surface, which had been extracted and tessellated from subjects' structural MRI data. To reduce the number of possible source locations, a smaller number of vertices were then down-sampled from the cortical surface as regularly as possible and used for source reconstruction purposes; whereas the original mesh information was used only for visualization purposes [10, 26]. In the present study, about 15,000 vertices were down-sampled from more than 400,000 original cortical vertices.

To reconstruct the cortically distributed brain sources, we used a linear estimation approach [6, 8]. The expression for the inverse operator \mathbf{W} is:

$$\mathbf{W} = \mathbf{R}\mathbf{A}^T(\mathbf{A}\mathbf{R}\mathbf{A}^T + \lambda^2\mathbf{C})^{-1}, \quad (1)$$

where \mathbf{A} is a lead field matrix that relates source locations to scalp electrodes, \mathbf{R} is a source covariance matrix, and \mathbf{C} is a noise covariance matrix. The source distribution can be estimated by multiplying the measured signal at a specific instant x by \mathbf{W} . If we assume that both \mathbf{R} and \mathbf{C} are scalar multiples of an identity matrix, this approach becomes identical to minimum

norm estimation [28]. In this study, the source covariance matrix \mathbf{R} was assumed to be a diagonal matrix, which means that we ignored the relationships between neighboring sources. The lead field weightings [16, 26] were imposed on the lead field matrix to compensate for the sensitivity difference according to the source depth. In this study, a pre-stimulus time window was used to calculate \mathbf{C} [26, 28]. λ^2 is a regularization parameter and was determined using the L-curve method [18].

The author imposed the fMRI constraint by giving different weighting values to the diagonal terms of \mathbf{R} . Without considering fMRI priors, \mathbf{R} is an identity matrix. When fMRI constraints were imposed, the diagonal terms of \mathbf{R} were set to 1 for source locations within fMRI activation regions, and 0.1 for source locations outside fMRI activation regions [27, 28] in order to minimize the distortion of source patterns stemming from both fMRI visible and invisible sources [27].

In the present study, a realistic geometry head model was used for accurate EEG forward calculation [17, 20]. A first order node-based boundary element method (BEM) was applied to construct the lead field matrix. Three-layer tessellated boundary surfaces, consisting of inner and outer skull boundaries and a scalp surface, were generated. For all realistic simulations performed in the present study, the MNI standard brain atlas (http://www.mrc-cbu.cam.ac.uk/Imaging/Common/mnispace.shtml#evans_proc) was utilized. The relative conductivity values of brain, skull, and scalp were assumed to be 1, 1/16, and 1, respectively [19, 32].

2.2 Modifying prior activation regions

As mentioned before, fMRI constrained EEG source imaging might result in incorrect EEG source estimates when the fMRI activation regions do not cover the actual EEG source locations. Figure 1a and b show schematic diagrams to elucidate the influence of false fMRI information. As depicted in Fig. 1a, the fMRI constrained inverse solution can be more focalized than the conventional linear inverse solution, when fMRI prior activation regions cover the actual source locations. As seen in Fig. 1b, however, fMRI constrained source imaging can cause distorted or false source estimates when there are severe mismatches between fMRI prior activation regions and actual neuronal source locations.

To tackle this problem, the author first reconstructed distributed EEG sources at every time slice of a complete time window without any functional a

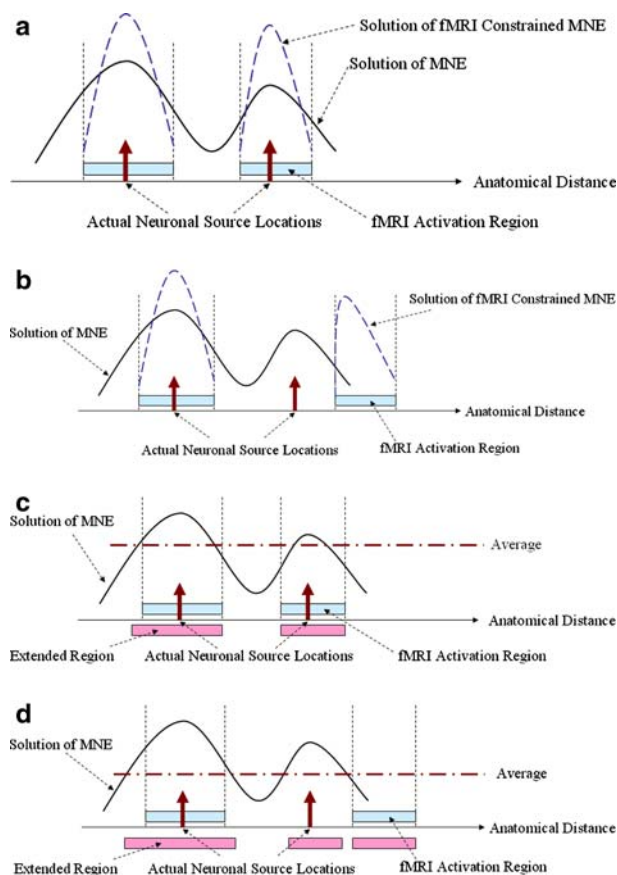


Fig. 1 Schematic diagrams to elucidate the influence of mismatch sources upon the estimated source images and the new technique concept **a** fMRI activation regions cover two actual source locations; **b** fMRI activation regions do not cover one of the neuronal source locations. Solutions of fMRI constrained source imaging might be distorted when a fMRI activation region cannot cover actual neuronal source locations; **c** when the fMRI activation regions cover all of the actual neuronal sources, the extension of the prior activation regions is slight because no significant activations exceeding Q_{AVE} are found outside of the fMRI activation regions; **d** when one significant missing source exists outside the fMRI activation regions, the neuronal source location is included in the new prior activation regions since the EEG or MEG source estimates around the neuronal source are significant enough to exceed the threshold value

priori information, and then calculated the ‘partial time integration’ value at every source point using:

$$J_i = \left\{ \max \left\{ \int_0^{\Delta t} j_i(t) dt, \int_{\Delta t}^{2\Delta t} j_i(t) dt, \dots, \int_{(n-1)\Delta t}^{n\Delta t} j_i(t) dt \right\} \right\}, \quad (2)$$

where J_i is the partially integrated source intensity at i th cortical vertex, $j_i(t)$ is the source intensity at time slice t , and Δt is the time interval when the entire time window is divided into n sub-windows. The time

interval Δt should be carefully determined by considering how short the signal duration can be. The parameter cannot be implicitly determined, but should be determined empirically according to the users’ experience. If a user wants to localize spike-like sources, the time interval should be as short as 10 ms. If a user does not want to consider the fMRI invisible sources, he can set the value to be the entire time window. In the present simulation, we set the interval at 30 ms, considering the simulated source patterns. More implicit or recommended values can be given after exhaustive simulation and experimental studies, which will be conducted in the future.

The author then calculated an average of the partially integrated source intensities, denoted as Q_{AVE} , for the cortical vertices that belong to the given fMRI activation regions. Then, the source points outside the given fMRI activation regions, of which the integrated source intensities exceeded Q_{AVE} , were included in the new prior activation regions, while preserving the original (given) fMRI activation regions. Figure 1c and d show schematic diagrams elucidating the present approach. If the approach is applied to an example as shown in Fig. 1a, where the fMRI activation regions cover all actual neuronal sources, the extension of the prior activation regions may not be considered because no significant activations exceeding Q_{AVE} are found outside the fMRI activation regions (Fig. 1c). Then, the resultant fMRI constrained EEG source estimates will not be very different from the conventional fMRI constrained source estimates. On the other hand, when the present approach is applied to an example as shown in Fig. 1b, where one significant missing source exists outside the fMRI activation regions, the regions around the missing source location are included in the new prior activation regions since the EEG source estimates around the neuronal source are significant enough to exceed the Q_{AVE} value (Fig. 1d). As shown in the figures, the use of the present approach may fail to yield a concentrated source distribution, which is one of the main advantages of fMRI constrained EEG source imaging. Instead of sacrificing the focalized source distribution, however, more accurate source locations can be identified [22].

The present approach can be used to correct fMRI invisible sources as well as fMRI discrepancy sources, but cannot correct fMRI extra sources. As mentioned before, the fMRI extra sources do not significantly affect the solution.

Fujimaki et al. [12, 13] applied a similar idea to fMRI-constrained MEG dipole source localization. They added candidates of fMRI invisible dipoles by MEG-only analysis and investigated the temporal

variation of the fMRI invisible and visible sources. Although the approach is different, their study indirectly supports the author’s idea of a distributed source approach.

3 Simulation results and discussions

Neuroelectromagnetic inverse problems (NIP) are hard to verify by in-vivo experiments because exact source locations inside a real human brain cannot be estimated *a priori*. For that reason, artificially constructed forward data have been widely used to validate NIP algorithms [23, 38]. Hence, in the present simulation study, artificially constructed EEG data assuming realistic conditions were used. 128 electrodes were attached to a participant’s scalp according to the extended 10–20 electrode system. To utilize anatomical information, the interface between white and gray matter was extracted from MRI T1 images of the MNI standard brain [7, 11] and tessellated into 865,712 triangular elements and 432,654 vertices, using *BrainSuite* developed in the University of Southern California [39].

For the present simulation study, we assumed the four cortical sources shown in Fig. 2, which were orientated perpendicular to the cortical surface. The temporal variations of the dipole intensities were assumed as follows:

Source 1:

$$J = -10^{-4}(t - 100)^2 + 1 \quad (0 \leq t < 200 \text{ ms})$$

$$= 0 \quad (200 \leq t < 400 \text{ ms})$$

Source 2:

$$J = -10^{-4}(t - 200)^2 + 1 \quad (100 \leq t < 300 \text{ ms})$$

$$= 0 \quad (0 \leq t < 100, 300 \leq t < 400 \text{ ms})$$

Source 3:

$$J = -10^{-4}(t - 300)^2 + 1 \quad (200 \leq t < 400 \text{ ms})$$

$$= 0 \quad (0 \leq t < 200 \text{ ms})$$

Source 4:

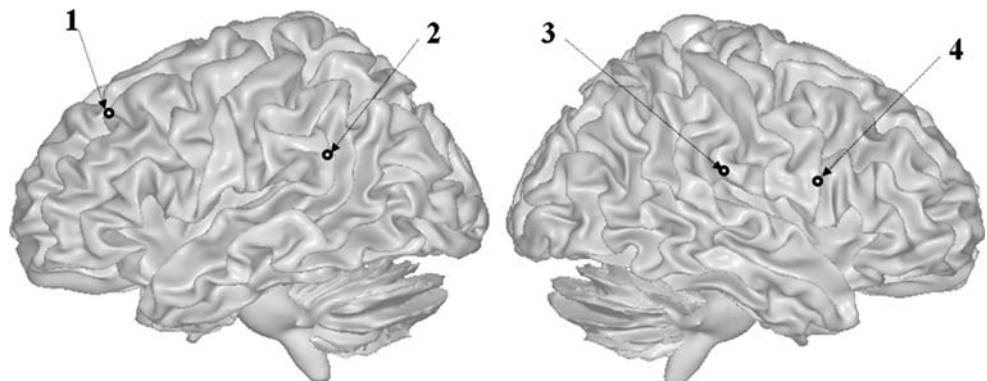
$$J = -1/9 \times 10^{-2}(t - 200)^2 + 1 \quad (170 \leq t < 230 \text{ ms})$$

$$= 0 \quad (0 \leq t < 170, 230 \leq t < 400 \text{ ms})$$

The locations and latencies of the assumed sources were arbitrarily chosen, i.e., their locations and latencies do not reflect any actual brain activations. After calculating electric potentials at every electrode assuming a 500 Hz-sampling rate, we added real background EEG signals starting from –400 ms, which were obtained from a pre-stimulus period of a practical EEG experiment. The original signal without noise was scaled so that the signal-to-noise ratio (SNR) was approximately 7 dB. The SNR was calculated as a ratio of powers between the signal time window (0–400 ms) and noise time window (–400 to 0 ms). The dipole intensities of the assumed sources did not require any physical unit because the author scaled the simulated EEG signal so that the SNR was 7 dB. Figure 3 shows the source waveforms and the artificial EEG signals with respect to time.

Before applying the present approach to the simulated EEG signals, we first reconstructed EEG source images using the conventional linear inverse operator without fMRI constraint at every time slice (from –400 to 400 ms). The time-varying source intensity at every cortical vertex was then partially integrated using (2) with $\Delta t = 30 \text{ ms}$, resulting in a possible significant source map shown in Fig. 4. We can see from the figure that the partially integrated source distribution correctly represents the rough locations of the presumed cortical sources. When the integration was performed for the entire time window, the activation around

Fig. 2 Locations of four cortical dipole sources assumed to simulate a realistic EEG signal



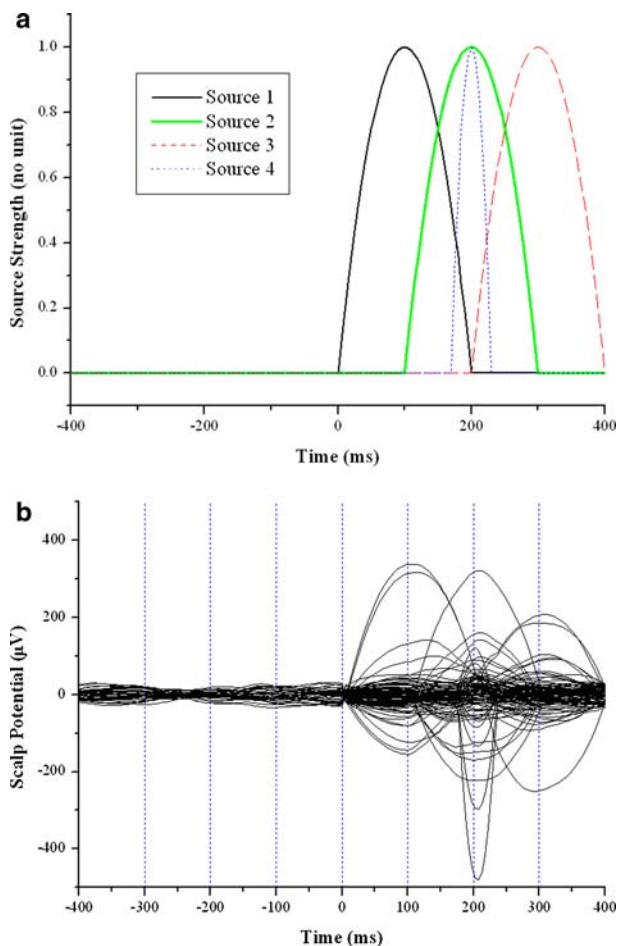


Fig. 3 Simulated source waveforms and EEG signals with a real background EEG signal (SNR = 7 dB) **a** assumed source waveforms; **b** simulated EEG signals

source four was not clear since the duration of the activation was relatively short.

In the present simulation study, five different cases of fMRI activation regions with similar areas were assumed as follows:

- Case 1: perfectly matching: all fMRI activation regions cover the actual EEG source locations.
- Case 2: one fMRI invisible source: there exists one fMRI invisible source—fMRI activation regions do not cover Source 4.
- Case 3: one fMRI discrepancy source: three fMRI activation regions cover actual EEG source locations (Sources 2, 3, and 4), but the other fMRI activation region does not cover Source 1.
- Case 4: two fMRI discrepancy sources: two fMRI activation regions cover the location of Sources 3 and 4, but the other two regions do not cover the actual source locations (Sources 1 and 2).
- Case 5: fMRI extra source: all fMRI activation regions cover the actual EEG source locations, but one fMRI activation region, which covers Source 1, has an extra area not relevant to an EEG source location.

The fMRI activation regions were produced independently regardless of the resultant EEG source images. After evaluating the Q_{AVE} , source points outside the original fMRI activation regions, of which the integrated source intensities exceeded the Q_{AVE} , were included in the new prior activation regions while maintaining the original fMRI activation regions. Figure 5 shows the comparison between original and modified prior activation regions, where newly added regions are filled with a different color. It can be seen from the figures that the prior activation regions were extended to include the missing EEG source locations, when there are significant mismatches between fMRI prior activation regions and actual EEG sources.

The author then compared the source distributions reconstructed at three time slices (100, 200, and 300 ms), under three different conditions: (1) no fMRI constraint; (2) with original fMRI prior activation regions; (3) with modified (extended) prior activation regions. Figure 6 shows the reconstructed source distributions for Case 1, where the normalized current

Fig. 4 Possible significant source map obtained from partial time integration of conventional source estimates

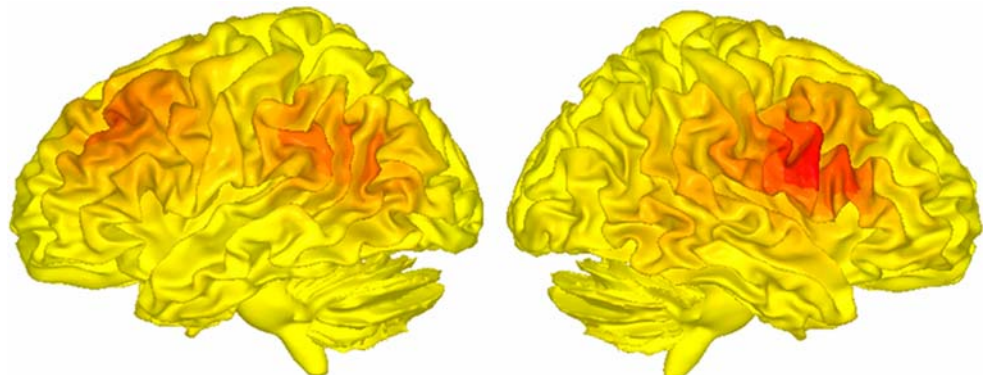


Fig. 5 Five different cases of fMRI activation regions and comparison with modified prior activation regions: Case 1: no mismatch source; Case 2: one fMRI missing source; Case 3: one fMRI discrepancy source; Case 4: two fMRI discrepancy sources; Case 5: one fMRI extra source. Please compare the fMRI activation locations with the actual source locations shown in Fig. 2. The numbers in the first column represent the number of cases. Cortical surfaces shown in second and third columns represent original and modified prior regions, respectively

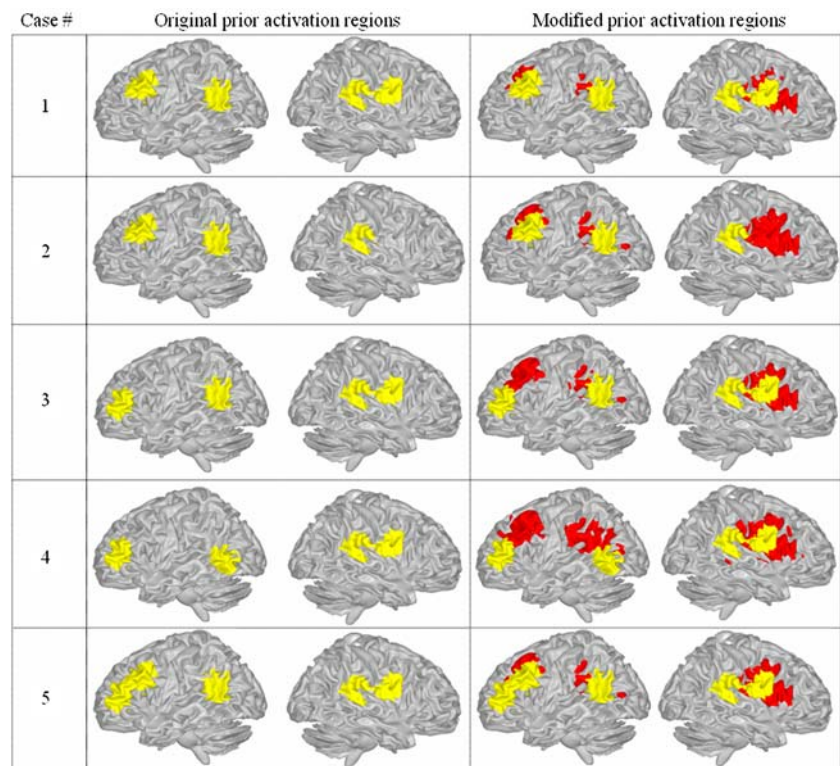
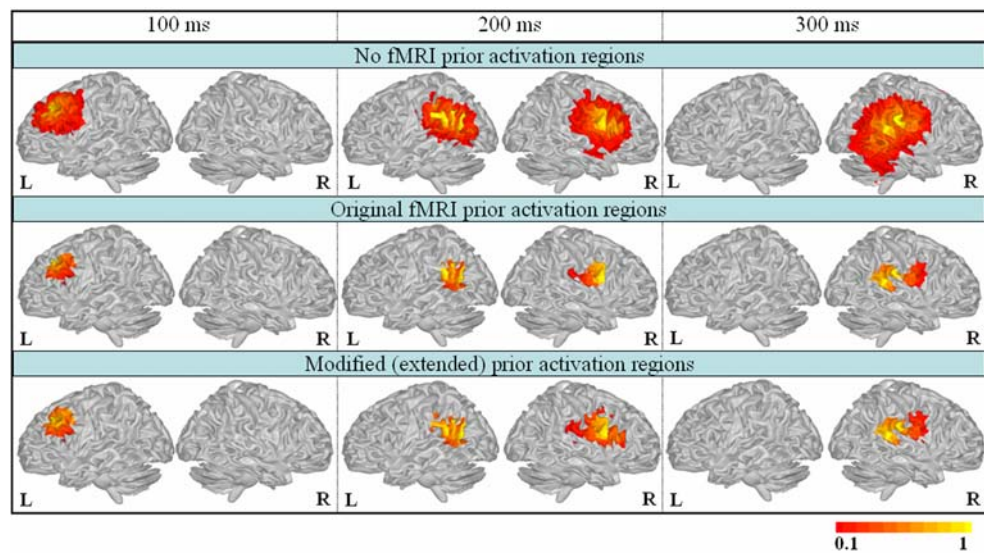


Fig. 6 Normalized current dipole power at 100, 200, and 300 ms, estimated for Case 1 under three different conditions (no fMRI information, with original prior activation regions, and with modified prior activation regions). Sources that exceed 0.1 are visualized. SNR = 7 dB

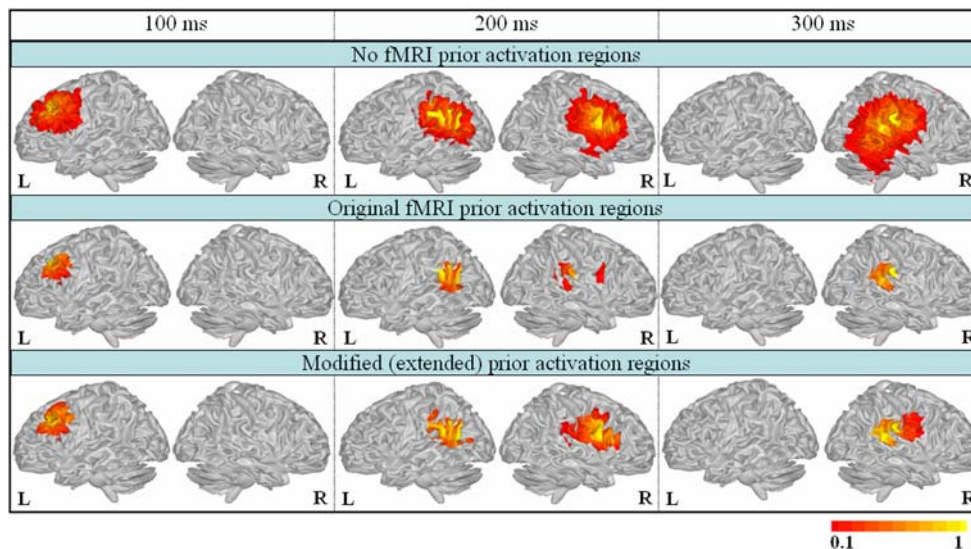


dipole power (the sum of squared dipole component strengths) was used for visualization purposes and small noisy sources with normalized power values below 0.1 were excluded from the visualization. The following facts can be observed from the figures: (1) More concentrated source distributions could be estimated by using the fMRI prior information as a functional constraint; (2) When the fMRI prior activation

regions cover all of the actual source locations, the source distributions estimated with modified prior activation regions were similar to those estimated with original prior activation regions, although somewhat extended activations were found around Source 4.

Figure 7 shows the source distributions reconstructed for Case 2, when there is one fMRI invisible source. From the figures, the following facts are

Fig. 7 Normalized current dipole power at 100, 200, and 300 ms, estimated for Case 2 under three different conditions (no fMRI information, with original prior activation regions, and with modified prior activation regions). Sources that exceed 0.1 are visualized. SNR = 7 dB



observable: (1) The fMRI constrained EEG source images estimated with original prior activation regions cannot properly detect the missing source location; (2) Although there is some loss in the concentration of the source distribution, we could identify the proper locations of Source 4 when the source images were reconstructed with modified prior activation regions.

Figures 8 and 9 show the source distributions reconstructed for Case 3 and Case 4, respectively, when one or two EEG sources are not matched with the original prior activation regions. As seen from the source estimates, the use of false fMRI information resulted in the severe distortion or misidentification of EEG source distributions. On the contrary, the use of modified prior regions resulted in more widespread source images compared to the original fMRI constrained source images, although we could identify the actual source locations more

appropriately. It was also observed that more mismatched sources yielded more widespread source distributions. Nevertheless, it seems obvious that widespread but reasonable source distribution is still more useful than the inaccurate source identification with focal distribution, in many practical applications.

Figure 10 shows the reconstructed source distributions for Case 5, when one fMRI activation region covers unnecessarily a vast area. These results show one possible drawback of the present approach. Since such extra fMRI activation regions reduce the value of Q_{AVE} , the modified prior activation regions become wider than that of the normal case (Case 1), resulting in more widespread source distributions. Nevertheless, this approach is thought to be still worthwhile because sacrificing focal source distribution to a certain extent is sometimes better than

Fig. 8 Normalized current dipole power at 100, 200, and 300 ms, estimated for Case 3 under three different conditions (no fMRI information, with original prior activation regions, and with modified prior activation regions). Sources that exceed 0.1 are visualized. SNR = 7 dB

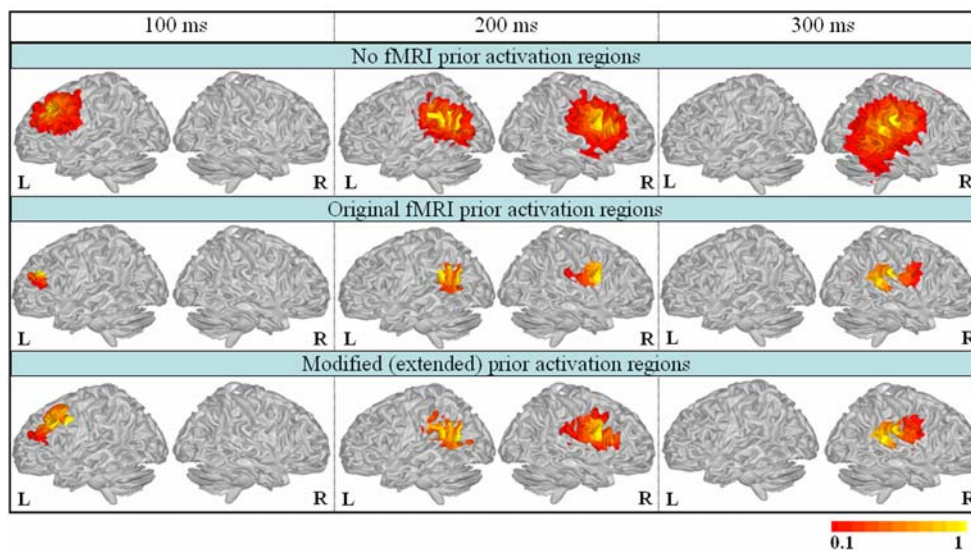


Fig. 9 Normalized current dipole power at 100, 200, and 300 ms, estimated for Case 4 under three different conditions (no fMRI information, with original prior activation regions, and with modified prior activation regions). Sources that exceed 0.1 are visualized. SNR = 7 dB

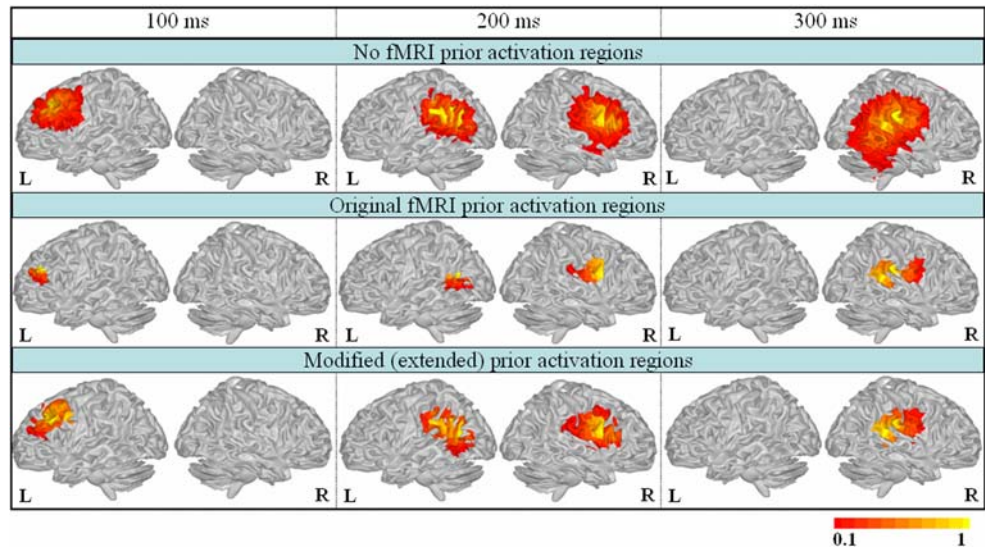
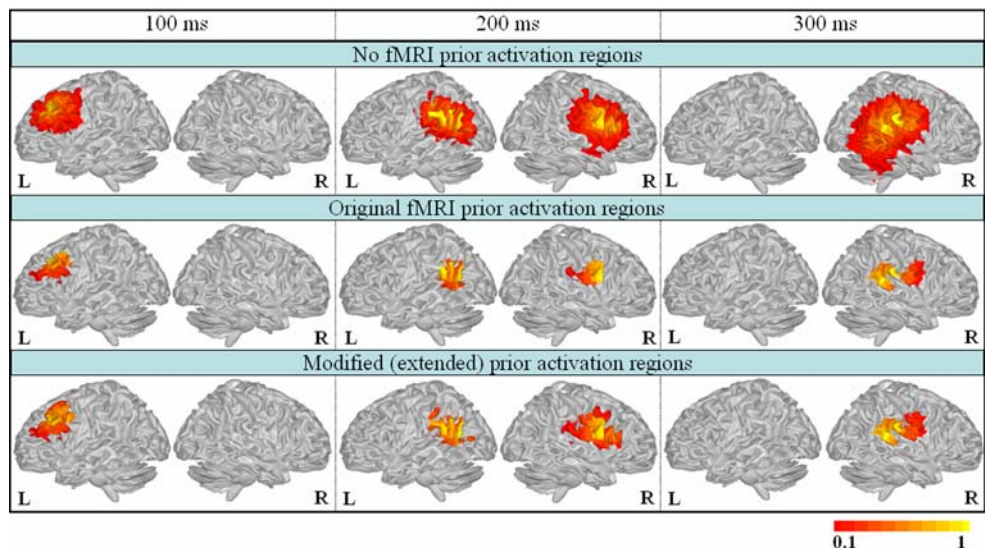


Fig. 10 Normalized current dipole power at 100, 200, and 300 ms, estimated for Case 5 under three different conditions (no fMRI information, with original prior activation regions, and with modified prior activation regions). Sources that exceed 0.1 are visualized. SNR = 7 dB



missing significant EEG source locations. Thus, the use of this approach is fully dependent upon the users’ choice, i.e., users should determine which result is more meaningful.

4 Discussions and conclusions

The present realistic simulation study demonstrates that significant mismatches between fMRI and EEG sources, which may cause misidentification of actual neuronal source locations, can possibly be considered in fMRI constrained EEG source imaging. This approach extended the prior activation regions by including significant EEG sources, of which the adjacent areas were identified by partial time integration of conventional source imaging results without

a priori information, into the modified prior activation regions. Such a strategy allows users to selectively apply the fMRI constraint to the EEG source imaging. In other words, the use of this approach rarely affects the results of conventional fMRI constrained EEG source imaging if no major mismatch between the two modalities is detected; while the new results become closer to those of typical EEG source imaging without an fMRI constraint if the mismatch level is significant.

The use of the present approach is fully dependent upon the users’ preferences. If a user gives high priority to obtaining a concentrated EEG source distribution with the aid of functional prior information, he has no need to apply the approach to the fMRI constrained EEG source imaging. However, he might fail to recover some significant fMRI invisible sources or estimate false source locations due to false fMRI

information. If the user aims to identify actual neuronal source locations and uses the fMRI functional information as an auxiliary tool to improve the specificity of the source images, the present approach can be a useful tool. As seen from the simulation results, some loss of concentration in the reconstructed source images may be inevitable if the new approach is adopted. Instead, he can identify the proper locations of fMRI invisible and discrepancy sources even when there are significant mismatches between the two modalities. Thankfully, the loss of focality was not significant when the mismatch level was not severe. Please note that even when there are two discrepancy sources, the estimated source images were still better than the ‘no-prior’ case (Fig. 9).

Nevertheless, there are some potential limitations that should be studied further. First, one should be careful when applying the present method to deep brain sources. Let us assume an fMRI prior region in the deep brain, within which the estimated source intensity using EEG alone is much weaker than in the superficial portions of the brain. The algorithm might end up with having significantly larger superficial cortical surface areas be included as the additional spatial priors or even extending the spatial priors onto the entire cortical surface. In such a case, deep fMRI activation will not help guide the imaging of deep electrical sources, which may be one of the most appealing features of using fMRI as a spatial constraint. Therefore, if one wants to apply the present approach to such a case, he should bear in mind that the benefits from the fMRI constrained EEG analysis might be lost. Conversely, if we assume that the fMRI prior region exactly covers one of the EEG sources in a very superficial cortical area, the average partial time integration within the fMRI prior region is likely to be greater than the partial time integration at any other source point, even with the existence of fMRI invisible sources at deeper locations. Therefore, the author recommends applying the present method to the superficial cortical sources as shown in the simulation studies.

Recently, some researchers have also tried to solve this mismatch problem. Sato et al. [37] used Bayesian estimation for the fMRI constrained MEG inverse solution and showed that their approach can reduce the influence of fMRI extra sources compared to the conventional Wiener estimation approach. Alfors [2] showed that use of two regularization parameters may reduce the influence of fMRI invisible sources on the reconstructed fMRI constrained MEG source images. More recently, Liu et al. [30] have shown that use of Twomey regularization may help to reduce the influ-

ence of fMRI invisible sources and fMRI extra sources. The three different approaches have shown that reducing the influence of mismatched sources may be possible to some extent. However, the recovery of fMRI invisible sources was not complete because they reduced the fMRI constraint strength in their ‘inverse operators’ when there were mismatches between fMRI and EEG (or MEG) source images. Thus, the recovered source strengths were much smaller than the actual ones. Contrary to their approach, the present approach extended the fMRI activation region to recover the mismatched EEG sources, resulting in complete recovery of the actual source strength. Similar to the present study, a loss of focal source distribution was also reported in previous works when the fMRI invisible source was considered in the inverse solution.

The present approach is an alternative technique to tackle technical problems in current multimodal neuroimaging methods. Ideally, more neuroscience studies should be conducted to reveal the origin of mismatch sources, which may enable us to understand the complex mechanisms of neuronal interactions and build a large-scale neural network model that can completely elucidate the differences between fMRI and EEG generators. The present study addresses fMRI constrained EEG source imaging, but it can also be applied to fMRI constrained MEG source imaging without any modifications since the inverse algorithms for EEG source imaging are identical to those for MEG source imaging. Further studies should be conducted to apply the present approach to more exhaustive simulations like the Monte-Carlo simulations and human in-vivo data analyses.

Acknowledgments This work was supported in part by a grant of the Korea Health 21 R&D project, Ministry of Health and Welfare, Korea (02-PJ3-PG6-EV07-0002), and in part by a grant (M103KV010016-06K2201-01610) from the Brain Research Center of the 21st Century Frontier Research Program funded by the Ministry of Science and Technology of the Republic of Korea.

References

1. Ahlfors SP, Simpson GV, Dale AM, Belliveau JW, Liu AK, Korvenoja A, Virtanen J, Huotilainen M, Tootell RBH, Aronen HJ, Ilmoniemi RJ (1999) Spatiotemporal activity of a cortical network for processing visual motion revealed by MEG and fMRI. *J Neurophysiol* 82:2545–2555
2. Ahlfors SP, Simpson GV (2004) Geometrical interpretation of fMRI-guided MEG/EEG inverse estimates. *NeuroImage* 22:323–332
3. Babiloni F, Babiloni C, Carducci F, Romani GL, Rossini PM, Angelone LM, Cincotti F (2003) Multimodal integration of high-resolution EEG and functional magnetic resonance imaging data: a simulation study. *NeuroImage* 19:1–15

4. Baillet S, Riera JJ, Marin G, Mangin JF, Aubert J, Garnero L (2001) Evaluation of inverse methods and head models for EEG source localization using a human skull phantom. *Phys Med Biol* 46:77–96
5. Bonmassar G, Schwartz DP, Liu AK, Kwong KK, Dale AM, Belliveau JW (2001) Spatiotemporal brain imaging of visual-evoked activity using interleaved EEG and fMRI recordings. *NeuroImage* 13:1035–1043
6. Dale AM, Sereno MI (1993) Improved localization of cortical activity by combining EEG and MEG with MRI surface reconstruction: a linear approach. *J Cognit Neurosci* 5:162–176
7. Dale AM, Fischl B, Sereno MI (1999) Cortical Surface-Based Analysis I. Segmentation and Surface Reconstruction. *NeuroImage* 9:179–194
8. Dale AM, Liu AK, Fischl BR, Buckner RL, Belliveau JW, Lewine JD, Halgren E (2000) Dynamic Statistical Parametric Mapping: Combining fMRI and MEG for High-Resolution Imaging of Cortical Activity. *Neuron* 26:55–67
9. Disbrow EA, Slutsky DA, Roberts TPL, Krubitzer LA (2005) Functional MRI at 1.5 tesla: A comparison of the blood oxygenation level-dependent signal and electrophysiology. *Proc Natl Acad Sci USA* 97:9718–9723
10. Dhond RP, Marinkovic K, Dale AM, Witzel T, Halgren E (2003) Spatiotemporal maps of past-tense verb inflection. *NeuroImage* 19:91–100
11. Fischl B, Dale AM (2000) Measuring the thickness of the human cerebral cortex from magnetic resonance images. *Proc Natl Acad Sci USA* 97:11050–11055
12. Fujimaki N, Hayakawa T, Nielsen M, Knösche TR, Miyachi S (2002) An fMRI-constrained MEG source analysis with procedures for dividing and grouping activation. *NeuroImage* 17:324–343
13. Fujimaki N, Hayakawa T, Matani A, Okabe Y (2004) Right-lateralized neural activity during inner speech repeated by cues. *Neuroreport* 15:2341–2345
14. George JS, Aine CJ, Mosher JC, Schmidt DM, Ranken DM, Schlitt HA, Wood CC, Lewine JD, Sanders J A, Belliveau JW (1995) Mapping Function in the Human Brain with Magnetoencephalography, Anatomical Magnetic-Resonance-Imaging, and Functional Magnetic-Resonance-Imaging. *J Clin Neurophysiol* 12:406–431
15. Gonzalez Andino SL, Blanke O, Lantz G, Thut G, Grave de Peralta Menendez R (2001) The Use of Functional Constraints for the Neuroelectromagnetic Inverse Problem: Alternatives and Caveats. *Int J Bioelectrom 3* (internet journal)
16. Gorodnitsky IF, George JS, Rao BD (1995) Neuromagnetic imaging with FOCUSS: a recursive weighted minimum norm algorithm. *Electroenceph Clin Neurophys* 95:231–251
17. Hämäläinen MS, Sarvas J (1989) Realistic conductivity geometry model of the human head for interpretation of neuromagnetic data. *IEEE Trans Biomed Eng* 36:165–171
18. Hansen P (1992) Analysis of discrete ill-posed problems by means of the L-curve. *SIAM Rev* 34:561–580
19. Haueisen J, Ramon C, Eiselt M, Brauer H, Nowak H (1997) Influence of tissue resistivities on neuromagnetic fields and electric potentials studied with a finite element model of the head. *IEEE Trans Biomed Eng* 44:727–735
20. He B, Musha T, Okamoto Y, Homma S, Nakajima Y, Sato T (1987) Electric dipole tracing in the brain by means of the boundary element method and its accuracy. *IEEE Trans Biomed Eng* 34:406–414
21. Im CH, Jung HK, Fujimaki N (2005) fMRI-constrained MEG source imaging and consideration of fMRI invisible sources. *Hum Brain Mapp* 26:110–118
22. Im CH, Lee SY (2006) A Technique to consider mismatches between fMRI and EEG/MEG sources for fMRI constrained EEG/MEG source imaging: a preliminary simulation study. *Phys Med Biol* 51:6005–6021
23. Kincses WE, Braun C, Kaiser S, Elbert T (1999) Modeling extended sources of event-related potentials using anatomical and physiological constraints. *Hum Brain Mapp* 8:182–193
24. Korvenoja A, Huttunen J, Salli E, Pohjonen H, Martinkauppi S, Palva JM, Lauronen L, Virtanen J, Ilmoniemi RJ, Aronen HJ (1999) Activation of multiple cortical areas in response to somatosensory stimulation: Combined magnetoencephalographic and functional magnetic resonance imaging. *Hum Brain Mapp* 8:13–27
25. Korvenoja A, Aronen HJ, Ilmoniemi J (2001) Functional MRI as a constraint in multi-dipole models of MEG data. *Int J Bioelectrom 3* (internet journal)
26. Lin FH, Witzel T, Hämäläinen MS, Dale AM, Belliveau JW, Stufflebeam SM (2004) Spectral spatiotemporal imaging of cortical oscillations and interactions in the human brain. *NeuroImage* 23:582–595
27. Liu AK, Belliveau JW, Dale AM (1998) Spatiotemporal imaging of human brain activity using functional MRI constrained magnetoencephalography data: Monte Carlo simulations. *Proc Natl Acad Sci USA* 95:8945–8950
28. Liu AK, Dale AM, Belliveau JW (2002) Monte Carlo simulation studies of EEG and MEG localization accuracy. *Hum Brain Mapp* 16:47–62
29. Liu Z, Ding L, He B (2006) Integration of EEG/MEG with MRI and fMRI in Functional Neuroimaging. *IEEE Eng Med Biol Mag* 25:46–53
30. Liu Z, Kecman F, He B (2006) Effects of fMRI-EEG mismatches in cortical current density estimation integrating fMRI and EEG: a simulation study. *Clinical Neurophysiology*, 117(7):1610–1622
31. Nunez PL, Srinivasan R (2005) *Electric Fields of the Brain : The Neurophysics of EEG*, 2nd Ed. Oxford University Press, Oxford
32. Oostendorp TF, Delbeke J, Stegeman DF (2000) The conductivity of the human skull: results of in vivo and in vitro measurements. *IEEE Trans Biomed Eng* 47:1487–1492
33. Opitz B, Mecklinger A, von Cramon DY, Kruggel F (1999) Combining electrophysiological and hemodynamic measures of the auditory oddball. *Psychophysiol* 36:142–147
34. Pascual-Marqui RD, Michel CM, Lehmann D (1994) Low resolution electromagnetic tomography: a new method for localizing electrical activity in the brain. *Int J Psychophysiol* 18:49–65
35. Phillips C, Mattout J, Rugg MD, Maquet P, Friston KJ (2005) An empirical Bayesian solution to the source reconstruction problem in EEG. *NeuroImage* 24:997–1011
36. Rothman DL, Sibson NR, Hyder F, Shen J, Behar KL, Shulman RG (1999) In vivo MRS studies of the relationship between glutamine-glutamine neurotransmitter cycle and functional neuroenergetics. *Phil Trans R Soc Lond B* 354:1165–1167
37. Sato MA, Yoshioka T, Kajihara S, Toyama K, Goda N, Doya K, Kawato M (2004) Hierarchical Bayesian estimation for the MEG inverse problem. *NeuroImage*, 23(3):806–826
38. Sekihara K, Nagarajan SS, Poeppel D, Marantz A, Miyashita Y (2001) Reconstructing spatio-temporal activities of neural sources using an MEG vector beamformer technique. *IEEE Trans Biomed Eng* 48:760–771
39. Shattuck DW, Leahy RM (2002) BrainSuite: An automated cortical surface identification tool. *Med Image Anal* 6:129–142

40. Torquati K, Pizzella V, Babiloni C, Gratta CD, Penna SD, Ferretti A, Franciotti R, Rossini PM, Romani GL (2005) Nociceptive and non-nociceptive sub-regions in the human secondary somatosensory cortex: An MEG study using fMRI constraints. *NeuroImage* 26:48–56
41. Vanni S, Warnking J, Dojat M, Delon-Martin C, Bullier J, Segebarth C (2004) Sequence of pattern onset responses in the human visual areas: an fMRI constrained VEP source analysis. *NeuroImage* 21:801–817
42. Vitacco D, Brandeis D, Pascual-Marqui R, Martin E (2002) Correspondence of event-related potential tomography and functional magnetic resonance imaging during language processing. *Hum Brain Mapp* 17:4–12
43. Wagner M, Fuchs M, Kastner J (2000) fMRI-constrained dipole fits and current density reconstructions. *Proc Bio-mag2000*